Journal of Applied Fluid Mechanics, Vol. 10, No. 1, pp. 117-126, 2017.
Available online at www.jafmonline.net, ISSN 1735-3572, EISSN 1735-3645.
DOI: 10.18869/acadpub.jafm.73.238.26366

Analysis of Interrupted Rectangular Microchannel Heat Sink with High Aspect Ratio

H. Kamal and A. Dewan†

Department of Applied Mechanics, Indian Institute of Technology Delhi, Hauz Khas, New Delhi - 110016, India

†*Corresponding Author Email: dewan_anupam@yahoo.com*

(Received March 31, 2016; accepted June 7, 2016)

ABSTRACT

A computational modelling of microchannel heat sinks with high aspect ratio has been performed to compare the geometrical features in the plane parallel to the heating surface and to determine the optimum configuration for the best heat transfer characteristics. A periodic thermal development of flow can cause significant heat transfer enhancement. A consensus on a particular geometrical configuration that provides the best heat transfer characteristics has not been reached in the literature, although many novel ideas have been proposed recently. Firstly the validity and applicability of microchannel sink modelling is presented followed by an optimization of parameters of interrupted microchannel heat sink. Consequences of the multichannel effect due to the introduction of transverse microchamber are also presented. It has been shown that the average Nusselt number of the microchannel heat sink increases by the introduction of a transverse microchamber with the additional advantage of a lower pressure drop. There exists an optimum width for the transverse microchamber for which the interrupted microchannel heat sink shows optimum characteristics.

Keywords: Microchannel heat sink; Heat transfer enhancement; Thermal redevelopment; Flow interruption.

1. INTRODUCTION

Ever since the introduction of semiconductor devices in the mid twentieth century, heat fluxes produced from microelectromechanical devices have been increasing exponentially due to decreasing size and increasing functionalities, especially in the recent decades. The conventional cooling methods have reached their upper limit in dissipating heat from such small volumes. Microchannel heat sinks have been proven to dissipate heat at far higher rate than the conventional devices due to their large heat transfer surface to volume ratio (Sobhan and Garimella, 2001). These are considered to be the choice of future cooling methods where heat is to be removed from very small surfaces with high heat fluxes (Tullius *et al.,* 2011; Zhang *et al.,* 2005; and Wang and Peng, 1994).

Cooling using micro channel heat sinks was first demonstrated by Tuckerman and Pease (1981). Heat flux up to 790 W/cm² was obtained by using the method. Recently Dewan and Srivastava (2015) presented a comprehensive review of studies dealing with heat transfer enhancement through flow disruption in microchannels. They concluded that a good amount of heat transfer augmentation can be achieved through flow disruption techniques, such as, shape of the channel, dimpled surfaces, ribs, cavities, groove structures, porous medium, etc. These techniques promote free-stream separation at the leading edge which results in the boundary-layer development and enhanced mixing leading to an increased heat transfer. Chai *et al.* (2016) numerically investigated and examined the characteristics of laminar flow and heat transfer in microchannel heat sink with the offset ribs on the sidewalls. Their results showed that the offset ribs result in significant heat transfer enhancement at the cost of a higher pressure drop.

Hong and Cheng (2009) presented a three-dimensional numerical study on laminar, forced convection of water in offset strip-fin microchannels network heat sinks for microelectronic cooling. The heat transfer and fluid flow characteristics in offset strip-fin microchannels heat sinks were analyzed and the heat transfer enhancement mechanism, effects of geometric size of strip-fin on the heat sink performance were investigated. They observed that there is an optimal strip-fin size to minimize the pumping power depending on the input heat flux and permitted maximum wall temperature. Chai *et al.* (2011, 2013) computationally investigated fluid flow

and heat transfer characteristics in a microchannel heat sink with offset fan-shaped reentrant cavities in sidewall and microchannel heat sink with periodic expansion-constriction cross sections. Their results indicated that the modified microchannel heat sinks improved heat transfer performance with an acceptable pressure drop. They observed that increased heat transfer surface area and periodic redevelopment of the hydraulic and thermal boundary-layers contributed to a significant heat transfer enhancement.

Xia *et al.* (2013) numerically investigated the behavior of water through the micro heat sink with fan-shaped reentrant cavities and internal ribs with different relative rib height for Reynolds number (*Re*) ranging from 150 to 600. They concluded that the new arrangement showed improved thermal performance at optimum ranges of parameters and *Re*. Xu *et al.* (2005) divided the whole flow length of microchannel heat sink into several independent zones, in which the thermal boundary-layer redeveloped periodically. They observed enhanced overall heat transfer along with decreased pressure drops for the newly proposed method compared to the conventional microchannel heat sink. Xu *et al.* (2008) and Munir *et al.* (2012) numerically simulated conjugate heat transfer in conventional and the interrupted microchannel heat sinks with triangular cross sections and studied the effects of changes in parameters, such as, total length and contact angle. They observed that flow rate variations in different channels were very small and can be neglected. They concluded that the repeated thermal developing flow enhances the overall heat transfer in microchannel heat sinks. Chai *et al.* (2013) introduced rectangular ribs in the transverse chamber in the microchannel heat sinks and optimized length and width of the rectangular ribs for the best heat transfer characteristics. They observed that notable effects of the new interrupted microchannel with rectangular ribs in the transverse microchambers on the mainstream flow are flow separation, recirculation or vortex and interrupted boundary-layer. Dang *et al.* (2012) performed numerical and experimental investigations to estimate the effect of gravity on the heat transfer and fluid flow phenomena of microchannel heat exchangers. They concluded that the effect of gravity can be ignored for numerical investigations.

From the aforementioned literature review, it can be deduced that periodic redevelopment of thermal boundary layer can result in a significant enhancement in microscale heat transfer. Gamrat *et al.* (2005) presented both two and three-dimensional numerical analysis of convective heat transfer in heat sink consisting of a very high aspect ratio rectangular microchannel. They concluded that two and three dimensional computations for the model used in the study were in perfect agreement.

In the present paper a two-dimensional computational simulation of high aspect ratio rectangular interrupted microchannels has been presented, which is shown to be suitable to study and analyze the effects of geometrical parameters along the plane of the microchannel heat sink. Two important implications of multichannel effect were observed. A significant heat transfer enhancement was observed in the interrupted microchannel heat sink with an additional advantage of lower pressure drop. The width of the transverse chamber introduced to induce flow separation is optimized for the best heat transfer characteristics.

2. MATHEMATICAL FORMULATION AND SOLUTION METHODOLOGY

2.1 3-D Modelling of Microchannel Heat Sink

To justify the usage of 2D computational analysis for high aspect ratio microchannel heat sinks, 3D simulations of simple microchannel with different aspect ratios were analyzed. 3D flow and heat transfer in a rectangular microchannel heat sink were studied computationally using water as the cooling fluid. The heat sink (Fig. 1) consisted of 10 mm long silicon substrate, which is used in electronics for the fabrication of integrated circuits. The micro-channels had a width of 57 μm and were separated by a 43 μm wall. Table 1 provides dimensions of single channel heat sink considered in the present study. The channel geometry considered in the present study was identical to that used by Kawano *et al*. (2001), Qu and Mudawar (2002), Fedorov and Vikasanta (2000), and Li *et al.* (2004), but with varied channel height to compare the effects of the aspect ratio. Due to the symmetry of the structure and repeating geometries, one unit cell (shown in Fig. 1) was considered and computationally simulated to analyze the microchannel heat sink. The walls at either side of the unit cell were assumed to be adiabatic. It was assumed that the electronic component emanated a uniform heat flux of 90 W/cm². The maximum theoretically possible heat flux to the ambient was found to be approximately 1% of the heat flux supplied at the bottom surface, assuming convection heat transfer coefficient for air ranging from 10 to 100 W/m^{2}K. Therefore the heat flux from the upper surface of the heat sink to the surroundings was neglected and there was no heat flux from the bottom surface either. The aspect ratio of the rectangular channel was changed gradually keeping the cross sectional area same to study the flow characteristics at high aspect ratios.

Table 1 Dimensions of single channel in the heat sink

W (μm)	W_w (μm)	D_h (μm)	L_y (μm)	L_z (μm)	L_x (mm)
57	43	86.58	900	100	10

The averaged longitudinal Nusselt number for three dimensional unit cell is defined as

$$\overline{Nu_x} = \frac{\overline{h_x}.D}{k_f} \quad (1)$$

where, $\overline{h_x}$ denotes the local heat transfer coefficient, D the hydraulic diameter and k_f the thermal conductivity of the fluid.

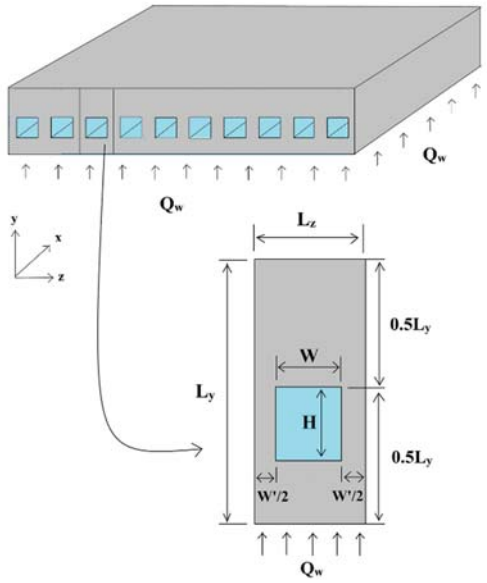

Fig. 1. Rectangular uninterrupted microchannel and the unit cell.

The longitudinal mean temperature difference in Eq. 1 is given as

$$\Delta\overline{T}(x) = \overline{T_w}(x) - \overline{T_b}(x) \tag{2}$$

here the local wall temperature averaged over the perimeter is given as

$$\overline{T_w}(x) = \frac{\sum^{w} T_w(i,j,k)}{N_w} \tag{3}$$

The longitudinal liquid bulk temperature is given as

$$\overline{T_b}(x) = \frac{\Sigma\,\Sigma \rho_f.\mathrm{u(j,k)}.C_p.T_b(\mathrm{i,j,k}).\Delta\mathrm{x}\Delta\mathrm{y}}{\dot{m}\,.C_p} \tag{4}$$

where ρ_f denotes the density of fluid, u the streamwise velocity of fluid, $\dot{m}$ the mass flow rate and C_p the specific heat capacity of fluid.

Effects due to gravitational force were neglected (Dang *et al.,* 2012). The flow was assumed to be three-dimensional, laminar and steady. The viscous dissipation was considered. The hydraulic diameter of the channel was 86 µm and *Re* ranged from 40 to 162. The governing equations for the fluid domain are

Continuity equation

$$\frac{\partial(\rho_f u_i)}{\partial x_i} = 0 \tag{5}$$

Momentum equation

$$\frac{\partial(\rho_f u_i u_j)}{\partial x_i} = -\frac{\partial p}{\partial x_j} + \frac{\partial}{\partial x_i}[\mu_f(\frac{\partial u_j}{\partial x_i} + \frac{\partial u_i}{\partial x_j})] \tag{6}$$

Energy equation

$$\frac{\partial\left(\rho_f u_i c_{pf} T\right)}{\partial x_i} = \frac{\partial}{\partial x_i}(\lambda_f \frac{\partial T}{\partial x_i}) + \mu_f[2\left(\frac{\partial u_i}{\partial x_i}\right)^2 + (\frac{\partial u_j}{\partial x_i} + \frac{\partial u_i}{\partial x_j})^2] \tag{7}$$

Energy equation for the solid part of microchannel

$$\frac{\partial}{\partial x_i}\left(k_s \frac{\partial T}{\partial x_i}\right) = 0 \tag{8}$$

Table 2 Thermal conductivity of silicon substrate (Incropera *et al.*, 2010).

Temperature K	200	250	300	350	400
Thermal conductivity W/m.K	264	191	148	119	98.9

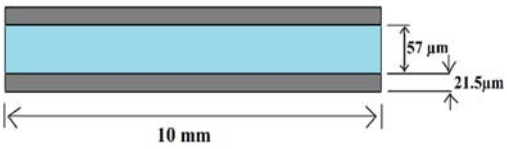

Fig. 2. Microchannel modelled in two dimension.

Table 3 Thermo-physical properties of water (Yang, 1998)

T K	P kg/m^3	C_p J/kg.K	K W/m.K	µ Pa.S
293	998.2	4183	0.599	0.001004
303	995.7	4174	0.618	0.0008015
313	992.2	4174	0.635	0.0006533
323	988.1	4174	0.648	0.0005494
333	983.1	4179	0.659	0.0004699
343	977.8	4187	0.668	0.0004061
353	971.8	4195	0.674	0.0003551
363	965.3	4208	0.680	0.0003149

Solutions to the above-mentioned governing equations were obtained using the commercial CFD solver FLUENT 15. The solutions were considered to be converged when the scaled residual values were less than 10^{-7} for all variables but 10^{-9} for the energy equation. The SIMPLE (Semi Implicit Method for Pressure Linked Equations) scheme (Patankar, 1980) was used for the pressure-velocity coupling. The second order upwind scheme (Barth and Jespersen, 1989) was used for the discretization. Temperature dependent thermo-physical properties of silicon substrate and water used are given in Tables 2 and 3.

2.2 2-D Modelling of Microchannel Heat Sink

To compare the flow features and heat transfer characteristics in 2D and 3D simulations, the same microchannel was also modelled in two dimensions. A channel of the same width and volume flow rate was considered. A schematic of 2D model is shown in Fig. 2. A heat generation of 11627.9 W/cm^3 was supplied to the solid part per unit height of the channel for equivalent heat removal rate from the unit area of the heating surface.

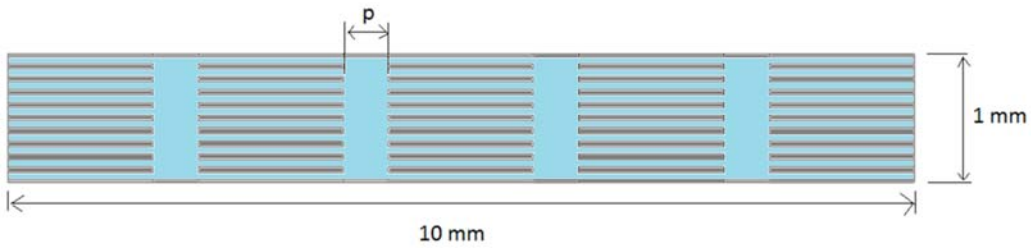

Fig. 3. Two dimensional modelling of interrupted microchannel heat sink with high aspect ratio

Table 4 Values of heat generation supplied for different transverse chamber widths to equate the total heat transfer rate per unit height

Width of transverse chamber, p (mm)	0.625	0.5	0.375	0.25	0.125
Heat flux given (W/cm^3)	16670.8	15756.0	14936.3	14197.7	13528.7

Similar to 3D model heat transfer to the ambient air was neglected. The same governing equations in 2D were considered. The thermo-physical properties of the solid part and fluid were assigned the same values. Only one channel was simulated due to the symmetry of the structure. Water at 290 K was supplied at the inlet for different flow rates.

2.3 2-D Modelling of Interrupted Microchannel Heat Sink

After comparison of 2D and 3D modelling of microchannel heat sink, interrupted microchannel heat sink with a high aspect ratio was considered to optimize the geometrical features in the plane parallel to lower heating surface.

The microchannel heat sink modelled in two dimension was split into five separated regions based on the following thermal entrance length calculation using the classical theory of fluid flow (Kays, 1980) by introducing four transverse microchambers:

$$L_{h,e} = 0.055 ReD_h \tag{9}$$

$$L_{t,e} = 0.055 RePrD_h \tag{10}$$

here $L_{h,e}$ represents the hydrodynamic entrance length and $L_{t,e}$ the thermal entrance length. It is clear from the literature review that thermally developing region in the microchannels has significantly high Nusselt number compared to the fully developed region (Xu *et al.,* 2008). Ten channels were considered for the simulation to account for the multichannel effect. Hence domain was 1 mm wide and 10 mm long. A schematic of the computational domain for interrupted microchannel is shown in Fig. 3. All the dimensions of fluid channels and solid wall are shown in Fig. 4. The width of the transverse chamber (p) was taken as a parameter and varied in all chambers simultaneously to analyze the effect of the separated flow length on heat transfer characteristics. A uniform heat flux from the bottom of the heat sink in 3D case was replaced with a uniform heat generation in the solid part. The values of the heat generation supplied for different transverse chamber widths (parameter p) to equate the total heat transfer rate per unit height in all cases are given in Table 4. Fluid at temperature 290K was supplied at the inlet and *Re* of flow was given values of 37, 79, 120 and 162 for the analysis. The hydraulic diameter of the channel was 114 μm. The average Nusselt number of the entire microchannel heat sink was calculated using the following expression

$$Nu_m = \frac{QD_h(C_{pout}T_{out} - C_{pin}T_{in})}{Nk_f A_w \Delta T_m} \tag{11}$$

$$\Delta T_m = T_{wm} - (T_{in} + T_{out}) \tag{12}$$

where Q denotes the mass flow rate through the heat sink, D_h the hydraulic diameter of the channel, N the number of channels, k_f the thermal conductivity of the fluid, C_p the specific heat capacity of fluid, A_w the area of wall inside the channel, T_{wm} the average temperature of thin heating film adjacent to wall.

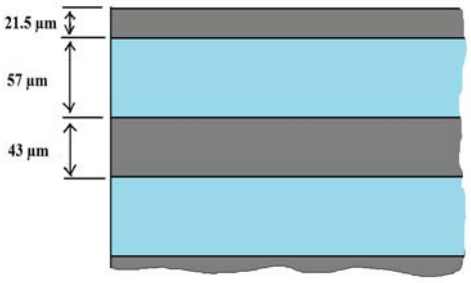

Fig. 4. Dimensions of fluid channels and solid walls in interrupted microchannel heat sink.

2.4 Grid Independence Study and Code Validation

The local Nusselt number averaged over the perimeter was observed to determine the grid independent solution for the microchannel unit cell modelled in three dimensions. Mesh was refined in all three directions independently. A fine mesh was

chosen for the transverse directions in order to properly resolve the velocity and viscous shear layers and to accurately define the conjugate heat transfer at the surface of the channel. A mesh with 180000 elements was found to be sufficient for the study.

Figure 5 shows variation of the Nusselt number in a very small length of the developing region of microchannel. Kawano *et al.* (2001) performed an experimental study using microchannels with the same dimensions as used in the present 3D computational study of microchannel. They defined the thermal resistance (R) of the microchannel as the ratio of the difference between the average temperature at the heated surface (T_s) and inlet (T_i) to the heat flux given at the bottom surface:

$$R = \frac{T_s - T_i}{q} \tag{13}$$

Figure 6 shows a comparison of R for different values of *Re* obtained in the present study compared with those of Kawano *et al.* (2001).

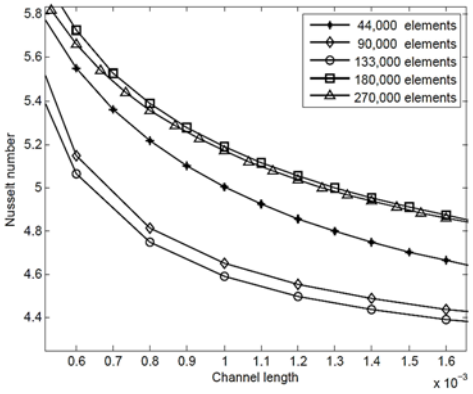

Fig. 5. Nusselt number observed for grid independence study.

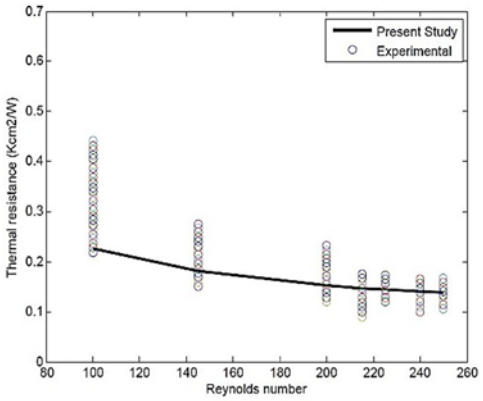

Fig. 6. Code validation by comparison with experimental study of Kawano *et al.* (2001).

3. RESULTS AND DISCUSSIONS

3.1 Comparison of 2-D and 3-D Simulations of High Aspect Ratio Microchannel Heat Sinks

Variations of streamwise velocity in the channel cross section and heat flux from the vertical side surfaces along the height of the channel were analyzed. The streamwise velocity was averaged in the horizontal direction and considered as a function of height from the bottom surface to study the effect of the aspect ratio. The aspect ratio was varied from 3.158 to 6.316, keeping the width of the channel constant. Figure 7 shows the variation of heat flux from the side wall at various heights of the channel for 3D and 2D models. H_m in Fig. 7 denotes the maximum height of the channel and H the height at which quantity is calculated by averaging along the horizontal direction. For a low aspect ratio, it could be seen from Fig. 7(a) that the heat flux values are different from each other at all heights. For the highest aspect ratio considered (6.316) the heat flux values showed similar values from the computational results for 2D and 3D simulations in 80% region of the vertical length of the channel. Therefore geometrical features in the plane parallel to heating surface can be compared and optimized using 2-D modelling.

Although actual optimized geometrical dimensions calculated in principle cannot be directly used for the manufacturing purposes, several geometrical features can be compared and optimum configuration for the best heat transfer characteristics can be obtained using 2D modelling. Similar observations can be made from the plot of streamwise velocity in the middle of microchannel and height of the channel (Fig. 8). Figure 8 shows that, apart from drop in values near the upper and lower walls, streamwise velocity showed nearly constant values for nearly 80% regions of the channel. Since heat transfer characteristics are functions of fluid velocity and heat flux values, it can be concluded that geometrical parameters in the horizontal plane can be compared and optimized using the computational model proposed.

3.2 2-D Analysis of Interrupted Microchannels

At the regions where transverse microchamber is present, microchannel flow behavior changes considerably. Changes in flow characteristics due to a combination of channels is called the multichannel effect. We have already observed from the literature that the introduction of transverse microchamber in microchannels can lead to better heat transfer characteristics (Xu *et al.*, 2008). But increasing the width of the transverse chamber after a certain extent can cause higher temperature in the silicon channel because of considerably reduced heat transfer surface area. Therefore, there has to be an optimum transverse chamber dimension at which the microchannel shows the best heat transfer characteristics. To calculate this dimension, the transverse chamber width (p) is taken as a parameter and varied continuously to observe heat transfer characteristics.

3.2.1 Multi-channel Effect

To carry out a 3-D analysis of interrupted microchannel heat sink, several studies ignored the multichannel effect and simulated only the repeating

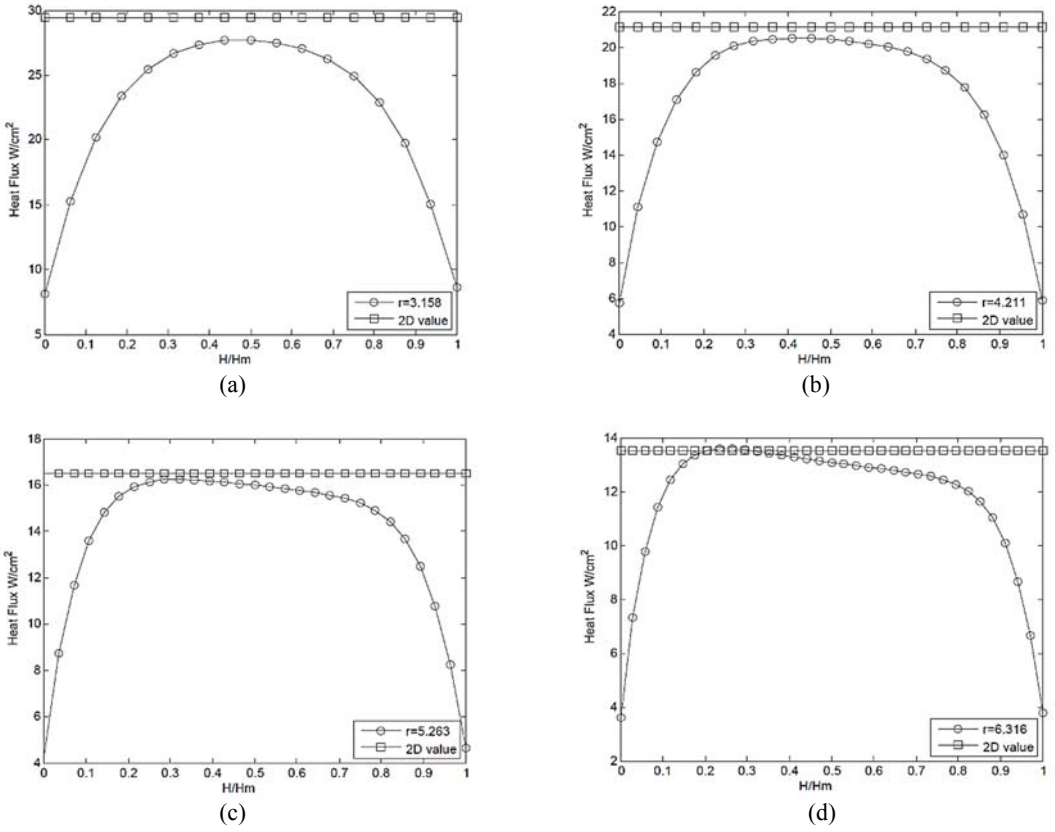

Fig. 7. Variation heat flux as a function of height from the bottom surface for aspect ratios (a) 3.158, (b) 4.211, (c) 5.263 and (d) 6.316.

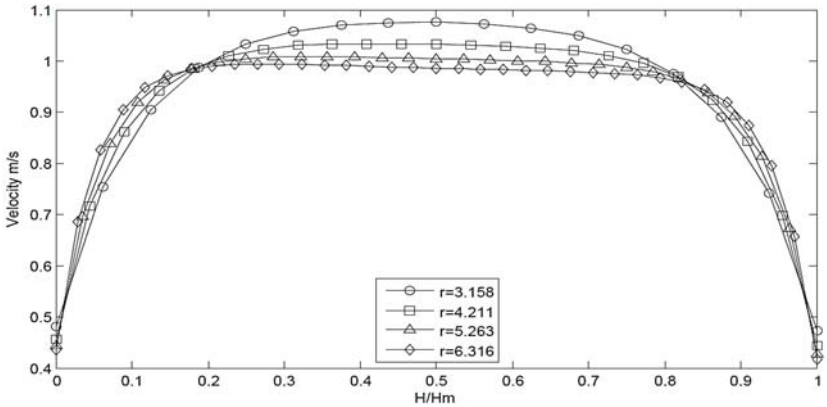

Fig. 8. Streamwise velocity along the height of the microchannel for different aspect ratios.

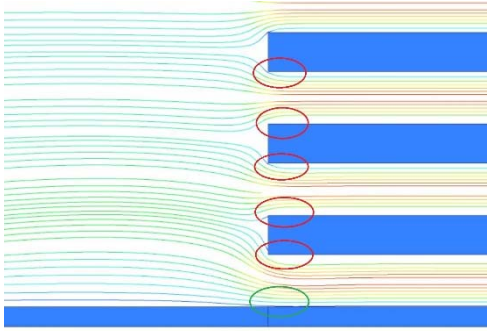

Fig. 9. Streamlines near the wall region.

geometry of microchannels (Wong and Lee, 2015; Chai *et al.,* 2013; and Hong and Cheng, 2009). A 2-D analysis provides the flexibility to analyze in detail the consequences of multichannel effect. There are two important consequences for multichannel flow with transverse chambers. At the regions where the channel walls are removed, i.e., at the transverse fluid chambers, microchannel tends to behave like a bigger channel whose hydraulic diameter is the combined width of the entire microchannel heat sink. This effect is more evident as the transverse chamber width is increased. At this region, friction from the wall causes lower fluid motion near the wall and

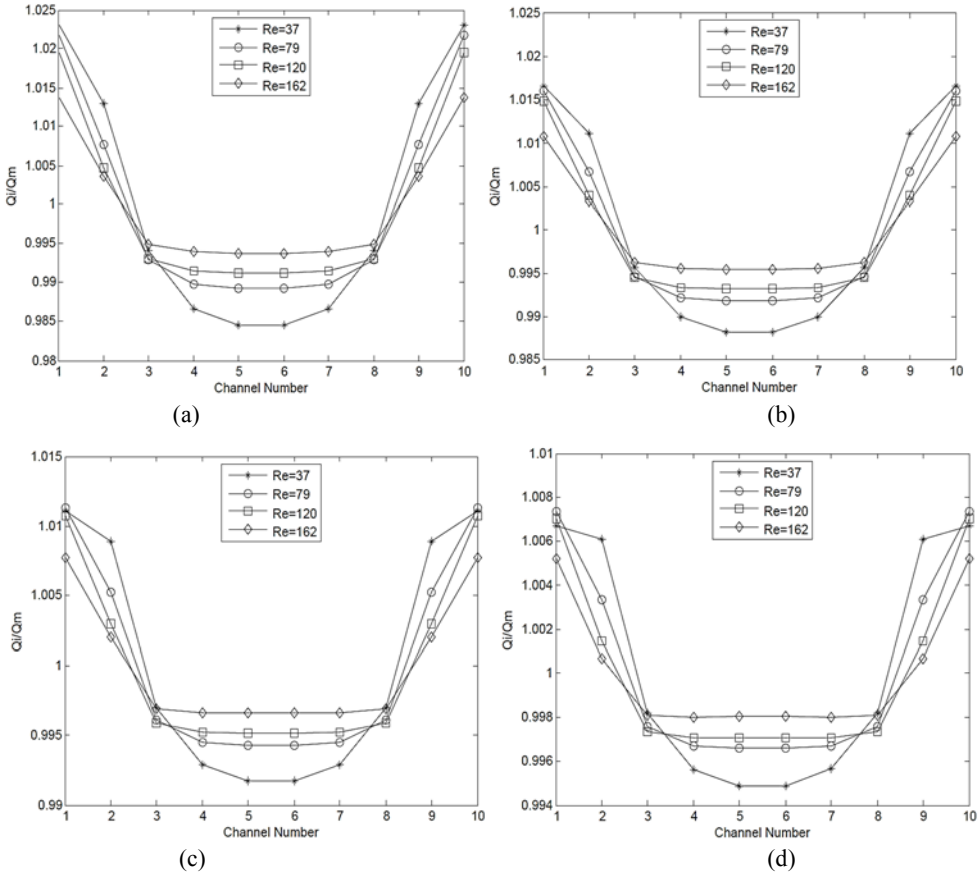

Fig. 10. Change in volume flow rate in different channels for transverse chamber widths (a) 0.625 mm, (b) 0.500 mm, (c) 0.375 mm and (d) 0.250 mm.

decreased fluid flow rate in the channels that are close to the wall. Therefore it causes higher fluid flow rate in the channels in the middle. The second effect is due to different kinds of entry and exit regions formed which influence the fluid motion from the transverse microchamber to channel and vice versa.

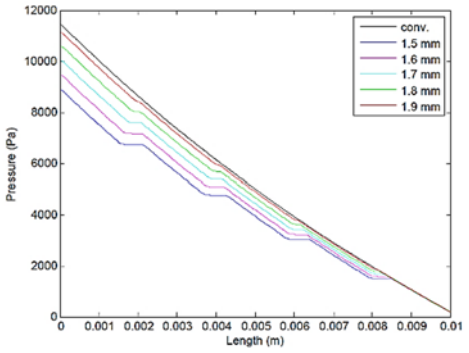

Fig. 11. Pressure variation along the length of the channel number 5 for *Re* = 79 for different separated channel lengths.

Unlike the entry regions of channels in the middle, streamlines do not have to abruptly change their directions for the channels at the extreme ends due to smooth entry. Hence vena contracta is not formed in those regions as marked in green circle in Fig. 9. The wall friction in the microchamber region results in sparsely spaced streamlines near the sidewalls. Consequently streamlines leading to the second channel also get pushed away resulting in lower effects due to vena contracta. Therefore effect due to entry region results in a higher volume flow rate in the channels at either extremes and lower volume flow rate in the channels in between with channel numbers 5 and 6 (refer Fig. 10) showing lowest volume flow rate. In the case presented in the present study, the effect due to entry regions dominates the effects due to combined channel flow. In the case presented by Xu *et al.* (2008), it can be seen that effects due to combined channel flow dominated the effect due to entry regions. The relative importance of these effects depends on the hydraulic diameter of the channel, cross sectional shape of the channel, aspect ratio, width of transverse chamber and *Re*. It is evident from Fig. 10 that the entrance effects clearly dominate the effect due to combined channel flow for lower *Re* considered. Here Q_i represents the volume flow rate in the n^{th} channel and Q_m represents the mean volume flow rate in channels. It can also be seen that for highest value of *Re* the behavior is significantly influenced by the effect due to

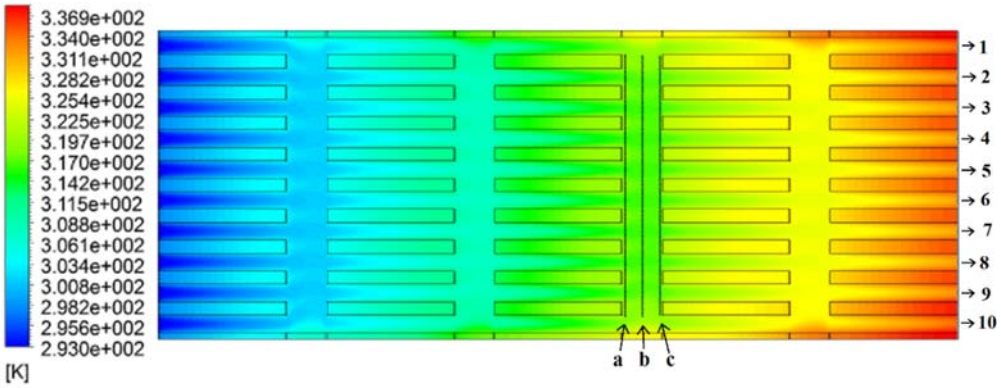

Fig. 12. Temperature contours of interrupted microchannel heat sink at *Re* = 79.

combined channel flow because of which volume flow rate in the middle channels is increased compared to those channels at lower *Re*. As the transverse chamber width is increased a mixed behavior is observed in the microchannel heat sink, channels at sides (1 and 10) and channels in the middle (5 and 6) being significantly influenced by the effect due to combined channel flow for the case with transverse chamber width 0.250 mm. Due to a mixed behavior the third and eighth channels had the lowest volume flow rate for that case with *Re* = 162.

3.2.2 Pressure and Temperature

Optimization was performed for four values of *Re* equal to 37, 79, 120 and 162 to study the effect of changing hydrodynamic entrance length and thermal entrance length. A very obvious consequence of using interrupted channels was considerably decreased pressure drop. Observed pressure drops for different simulation runs with varying transverse microchamber width (separated channel length used as legends in Fig.11 and 13) for *Re* of 79 are shown in Fig. 11. The pressure drop decreased considerably for interrupted channels in all cases. Therefore it can be concluded that even if heat transfer characteristics have not improved significantly, interrupted channel will still be of high significance due to its advantage of a reduced pressure drop in the channel. A gain in the pressure drop is directly proportional to the width of transverse microchamber. This gain in pressure drop is due to a decrease in the friction offered by the walls for the reduced channel length. Pressure head losses due to the exit from the channel to mircrochamber and re-entry to microchannel are much smaller in magnitude compared to the gain due to a reduced channel length. Fig. 12 also shows the temperature contour plot for *Re* = 79.

Since silicon microchannel is directly in contact with electronic component, it is important to analyze the temperature variations along the length of the channel. Temperature variations along the walls of the channel number 5 for *Re* = 162 in uninterrupted channel and different cases of uninterrupted channel are shown in Fig. 13. It can be seen that temperature of interrupted channel is higher than that of uninterrupted channel for the first three separated channel sections. Temperature in interrupted channel walls was less than or slightly greater than that of uninterrupted (marked as "conv." in Fig. 13) channels for last two separated channel sections.

3.2.3 Optimization of Transverse Chamber Width

An optimization of the transverse chamber width was performed to find the geometrical parameters at which microchannel heat sink shows the best heat transfer characteristics. Convective heat transfer characteristics of a surface is best described by the Nusselt number. Interrupted microchannels showed good heat transfer characteristics as transverse chamber width is increased, up to a certain extent after which it showed poorer characteristics.

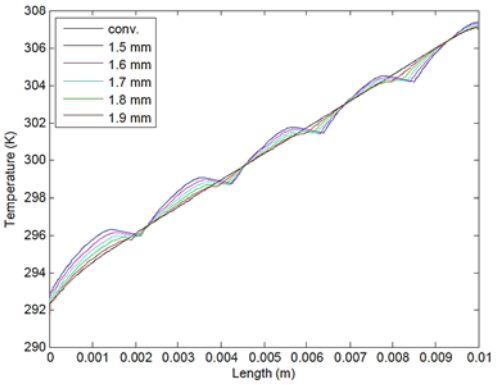

Fig. 13. Temperature variation along the walls for channel number 5 for *Re* = 162.

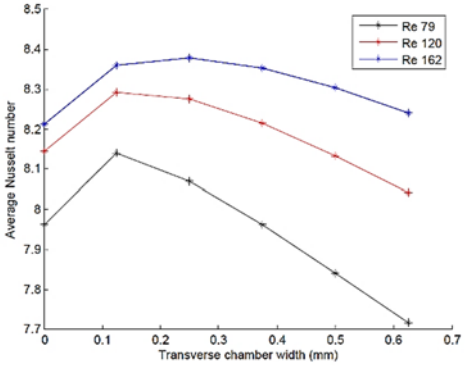

Fig. 14. Optimization of transverse chamber width.

It is observed from Fig. 14 that, for *Re* = 162, the average Nusselt number for the entire microchannel heat sink increased for the transverse chamber width from 0 to 0.25 mm after which it decreased. Such an optimum value for the transverse chamber width for Nusselt number was observed for all cases. Bigger the *Re*, higher the transverse chamber width required for the best thermal performance.

Approximately 5% increase in the average Nusselt number for the entire heat sink was observed for ranges of *Re* chosen for an optimum transverse chamber width (Fig. 14). This gain in *Nu* came along with 3% to 7% decrease in the pumping pressure requirement.

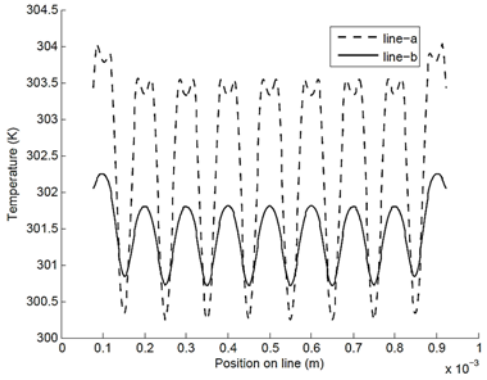

Fig. 15. Temperature at line-a and line-b.

Xu *et al.* (2008) concluded that repeated thermal developing flow enhances heat transfer in heat sinks where thermal redevelopment is much slower than hydrodynamic redevelopment. Figure 15 shows the temperature of fluid when it leaves the microchannels to microchamber (line-a, refer Fig. 12) and when it re-enters the microchannels. Although microchamber brought down temperature variation along the line significantly, redevelopment is not complete. It still has a temperature variation of about 1 K. This variation can be further brought down by the introduction of vertical structures which can enhance the mixing in the microchamber, leading to even better thermal performance.

4. CONCLUSIONS

(1) Using periodically interrupted microchannel heat sink can result in a significant heat transfer enhancement along with lower pressure penalty.

(2) There exists an optimum width of the transverse chamber for interrupted microchannels where thermal performance is maximum.

(3) Two dimensional modelling of microchannel heat sink can help us determine the best geometrical configuration for which the thermal performance is optimum.

(4) There are two major consequences of multichannel flow in interrupted microchannel heat sink. First is due to the combined channel flow in transverse microchambers. Second is due to entrance effects. Relative significance of these effects depends on flow and geometrical parameters.

REFERENCES

Barth, T. J. and D. Jespersen (1989). The design and application of upwind schemes on unstructured meshes. *Technical Report AIAA-89-0366, AIAA 27th Aerospace Sciences Meeting,* Reno, Nevada.

Chai, L., G. D. Xia and H. S. Wang (2016). Numerical study of laminar flow and heat transfer in microchannel heat sink with offset ribs on sidewalls. *Appl. Therm. Eng.* 92, 32-41.

Chai, L., G. Xia, L. Wang, M. Zhou and Z. Cui (2013). Heat transfer enhancement in microchannel heat sinks with periodic expansion-constriction cross-sections. *Int. J. Heat Mass Transf.* 62, 741-751.

Chai, L., G. Xia, M. Zhou and J. Li (2011). Numerical simulation of fluid flow and heat transfer in a microchannel heat sink with offset fan-shaped reentrant cavities in sidewall. *Int. Commun. Heat Mass Transf.* 38, 577–584.

Chai, L., G. Xia, M. Zhou, J. Li and J. Qi (2013). Optimum thermal design of interrupted microchannel heat sink with rectangular ribs in the transverse microchambers. *Appl. Therm. Eng.* 51, 880-889.

Dang, T., N. Tran and J. Teng (2012). Numerical and experimental investigations for effect of gravity to the heat transfer and fluid flow phenomena of microchannel heat exchangers. *Int. J. of Computational Engineering Research* 2(2), 260-270.

Dewan, A. and P. Srivastava (2015). A review of heat transfer enhancement through flow disruption in a microchannel. *J. Therm. Sci.* 24, 203-214

Fedorov, A. G. and R. Viskanta (2000). Three-dimensional conjugate heat transfer in the microchannel heat sink for electronic packaging. *Int. J. Heat Mass Transf.* 43, 399-415.

Gamrat, G., M. Favre-Marinet and D. Asendrych (2005). Conduction and entrance effects on laminar liquid flow and heat transfer in rectangular microchannels. *Int. J. Heat Mass Transf.* 48, 2943-2954.

Hong, F. and P. Cheng (2009). Three dimensional numerical analyses and optimization of offset strip-fin microchannel heat sinks. *Int. Commun. Heat Mass Transf.* 36, 651-656.

Incropera, L. and B. De Witt (2010). *Fundamentals of Heat And Mass Transfer.* 6th ed., Wiley India Pvt Ltd.

Kawano, K., M. Sekimura, K. Minakami, H. Iwasaki and M. Ishizuka (2001). Development of micro channel heat exchanging. *The Japan Society of*

Mechanical Engineers. International Journal Series B. 44, 592-598.

Kay, M. and M. E. Crawford (1980*). Convective Heat and Mass Transfer.* McGraw Hill, New York.

Li, J., G. P. Peterson and P. Cheng (2004). Three-dimensional analysis of heat transfer in a micro-heat sink with single phase flow. *Int. J. Heat Mass Transf.* 47, 4215-4231.

Munir, F. A., M. I. M Azmi, N. Razali and E. M. Tokit (2012). The effect of parameter changes to the performance of a triangular shape interrupted microchannel heat sink. *J. Teknol. Sciences Eng.* 58, 33–37.

Patankar, S. V. (1980). *Numerical Heat Transfer and Fluid Flow.* Taylor & Francis.

Qu, W. and I. Mudawar (2002). Analysis of three-dimensional heat transfer in micro-channel heat sinks. *Int. J. Heat Mass Transf.* 45, 3973–3985

Tuckerman, D. B. and R. F. W. Pease (1981). High-performance heat sinking for VLSI. *IEEE Electron Device Lett.* 2, 126-129.

Tullius, J. F., R. Vajta and Y. Bayazitoglu (2011). A Review of Cooling in Microchannels. *Heat Transfer Engineering* 32 (7–8), 527–541.

Wang, B. X. and X. F. Peng (1994). Experimental investigation on liquid forced convection heat transfer through microchannels. *International Journal of Heat and Mass Transfer* 37, 73-82.

Wong, K. C. and J. H. Lee (2015). Investigation of thermal performance of microchannel heat sink with triangular ribs in the transverse microchambers. *Int. Commun. Heat Mass Transf.* 65, 103–110.

Xia, G., Y. Zhai and Z. Cui (2013). Numerical investigation of thermal enhancement in a micro heat sink with fan-shaped reentrant cavities and internal ribs. *Appl. Therm. Eng*. 58, 52–60.

Xu, J. L., Y. H. Gan, D. C. Zhang and X. H. Li (2005). Microscale heat transfer enhancement using thermal boundary layer redeveloping concept. *Int. J. Heat Mass Transf.* 48, 1662-1674.

Xu, J., Y. Song Y., W. Zhang, H. Zhang and Y. Gan (2008). Numerical simulations of interrupted and conventional microchannel heat sinks. *Int. J. Heat Mass Transf.* 51, 5906-5917.

Yang, W. Q. T. S. M. (1998). *Heat Transfer.* 3rd ed., Higher Education Press, Beijing.

Zhang, H. Y., D. Pinjala, M. K. Iyer, R. Nagarajan, Y. K. Joshi, T. N. Wong and K. C. Toh (2005). Assessments of Single-Phase Liquid Cooling Enhancement Techniques for Microelectronics Systems. *In Proceeding ASME/Pacific Rim Technical Conference and Exhibition on Integration and Packaging of MEMS, NEMS, and Electronic Systems: Advances in Electronic Packaging*, San Francisco, CA, PART A, 43–50.